Mandibular molar root and pulp cavity morphology in *Homo naledi* and other Plio-Pleistocene hominins

Kornelius Kupczik[a, *], Lucas K. Delezene[b, c], Matthew M. Skinner[c, d, e]

[a] *Max Planck Weizmann Center for Integrative Archaeology and Anthropology, Max Planck Institute for Evolutionary Anthropology, Deutscher Platz 6, 04103 Leipzig, Germany*

[b] *Department of Anthropology, University of Arkansas, 330 Old Main, Fayetteville, AR, 72701, USA*

[c] *Evolutionary Studies Institute and Centre for Excellence in PaleoSciences, University of the Witwatersrand, South Africa*

[d] *School of Anthropology and Conservation, University of Kent, Canterbury, UK*

[e] *Department of Human Evolution, Max Planck Institute for Evolutionary Anthropology, Leipzig, Germany*

[*]Corresponding author.

E-mail address: kornelius_kupczik@eva.mpg.de (K. Kupczik).

Keywords: Tooth root morphology; Root canal morphology; *Homo* sp.; *Australopithecus africanus*; *Paranthropus robustus*; *Paranthropus boisei*

Abstract

The craniomandibular morphology of *Homo naledi* shows variable resemblances with species across *Homo*, which confounds an easy assessment of its phylogenetic position. In terms of skull shape, *H. naledi* has its closest affinities with *Homo erectus*, while mandibular shape places it closer to early *Homo*. From a tooth crown perspective, the smaller molars of *H. naledi* make it distinct from early *Homo* and *H. erectus*. Here, we compare the mandibular molar root morphology of six *H. naledi* individuals from the Dinaledi Chamber to those of African and Eurasian Plio-Pleistocene fossil hominins (totalling 183 mandibular first, second and third molars). The analysis of five root metric variables (cervical plane area, root length, root cervix volume, root branch volume, and root surface area) derived from microCT reconstructions reveals that the molar roots of *H. naledi* are smaller than those of *Homo habilis*, *Homo rudolfensis*, and *H. erectus*, but that they resemble those of three *Homo* sp. specimens from Swartkrans and Koobi Fora in size and overall appearance. Moreover, though *H. naledi* molar roots are similar in absolute size to Pleistocene *Homo sapiens*, they differ from *H. sapiens* in having a larger root volume for a given cervical plane area and less taurodont roots; the root cervix-to-branch proportions of *H. naledi* are comparable to those of *Australopithecus africanus* and species of *Paranthropus*. *Homo naledi* also shares a metameric root volume pattern ($M_2 > M_3 > M_1$) with *Australopithecus* and *Paranthropus* but not with any of the other *Homo* species ($M_2 > M_1 > M_3$). Our findings therefore concur with previous studies that found that *H. naledi* shares plesiomorphic features with early *Homo*, *Australopithecus*, and *Paranthropus*. While absolute molar root size aligns *H. naledi* with *Homo* from North and South Africa, it is distinguishable from these in terms of root volumetric proportions.

Introduction

Homo naledi, from the late Middle Pleistocene of South Africa, is characterized by a mosaic of ancestral and derived craniodental and postcranial anatomical features (Berger et al., 2015; Hawks et al., 2017 and references therein). Despite its relatively recent date of 236–335 ka (Dirks et al., 2017; Hawks et al., 2017), *H. naledi* retains a number of presumably ancestral features shared with eastern and southern African early *Homo*, *Australopithecus*, and *Paranthropus* (e.g., small body size, small brains both absolutely and relative to body size, curved manual phalanges, absence of styloid process on the third metacarpal, distally increasing mandibular molar size gradient, posteriorly directed humeral head, and flared ilium; Berger et al., 2015; Kivell et al., 2015; Feuerriegel et al., 2017; Garvin et al., 2017; VanSickle et al., 2017). In other anatomical characteristics (e.g., limb proportions, minimal body size dimorphism, proximal carpal anatomy, foot morphology) it shares derived features with *Homo sapiens*, *Homo heidelbergensis*, and *Homo neanderthalensis* (Harcourt-Smith et al., 2015; Kivell et al., 2015; Garvin et al., 2017). Analyses of skull morphology have yielded conflicting signals; a study of cranial shape suggests that *H. naledi* is phenetically similar to *H. erectus* (Laird et al., 2017), while an analysis of mandibular shape places *H. naledi* more closely with basal *Homo* (i.e., *Homo habilis*; (Schroeder et al., 2017). Thus, the phylogenetic place of *H. naledi* remains ambiguous (Dembo et al., 2016), but the emerging picture is one of a taxon that overlaps in time and possibly space with early *H. sapiens* but remains anatomically distinct. Such anatomical differences hint at possible marked ecological and behavioral differences between *H. sapiens* and *H. naledi*.

From a dental perspective, *H. naledi* has fairly small postcanine teeth with simple, crenulation-free crowns, lacking mass additive traits (Berger et al., 2015; Irish et al., 2018). The mandibular molar crown area gradient is $M_1 < M_2 < M_3$ (Berger et al., 2015; Hawks et al., 2017), which is the generally observed pattern in early hominins, including *H. habilis* (Evans et al., 2016). Yet, its

mandibular first molar crowns are buccolingually narrower than those of *Australopithecus sediba*, *H. habilis*, *Homo rudolfensis*, and early *H. erectus* (from Africa and Georgia; (Berger et al., 2015; Hawks et al., 2017). The mandibular premolars are somewhat molarized, with an expanded talonid, uniformly two-rooted P_3, and variably two-rooted P_4, which distinguishes *H. naledi* from *H. habilis* (see Berger et al., 2015). Likewise, the mandibular premolars of *H. erectus* from Georgia (P_3) and *Homo antecessor* from Spain (P_3 and P_4) are also said to be two-rooted (Bermúdez de Castro et al., 1999, 2014). The anterior teeth (incisors and canines) of *H. naledi* have crown and root dimensions most similar to those of modern *H. sapiens* and are smaller than those of early *Homo* (Le Cabec et al., 2017).

Tooth root morphology in fossil hominins

The external and internal morphology of both anterior (incisors and canines) and postcanine tooth (premolars and molars) roots has been used to unravel the taxonomic status of, and the phylogenetic relationships among, fossil hominins (Abbott, 1984; Wood et al., 1988; Kupczik and Hublin, 2010; Emonet et al., 2012; Le Cabec et al., 2013; Emonet et al., 2014; Moore et al., 2016). In particular, the assessment of the number and configuration of mandibular premolar roots has revealed two distinct P_3 morphoclines in hominins deriving from the ancestral form with a circular mesiobuccal root and a buccolingually extended distal root (Wood et al., 1988). Generally, while *H. erectus* and modern humans, as well as *P. robustus*, have simplified and reduced P_3 roots, *Paranthropus boisei* has molar-like P_3 roots (Wood, 1988). However, more recent studies have demonstrated that there is considerable variation in premolar root morphology within a single species and even within an individual (Kupczik et al., 2005; Shields, 2005; Moore et al., 2015; Moore et al., 2016), which would argue against the unrestricted validity of this trait in phylogenetic studies.

In this regard, molar root morphology appears to be more useful as at least the number of roots is less variable than that of premolars. Generally, the mandibular molars of hominins have two separated blade-like roots. In some modern human populations, high occurrences of three-rooted mandibular first molars (the mesial and distal roots plus a distinct distolingual accessory root) have been reported (e.g. Turner, 1971; Scott et al., 2018). Sperber (1974) also noted three-rooted M_3 in two South African hominin specimens (*P. robustus* SK841b with an accessory mesiobuccal root and *A. africanus* TM1518 with an accessory mesiolingual root. In the majority of two-rooted mandibular molars, both mesial and distal root portions are flattened mesiodistally, but the mesial root is buccolingually broader than the distal. In *P. robustus* from Swartkrans, the mesial root of the M_1 has been described to be larger than the distal one, while the opposite is the case for the M_2 (Robinson, 1956; Sperber, 1974). There are no reported root length data for the *P. robustus* M_3, but the mesial root was described to be directed vertically downward, while the distal root points distally and tapers (Robinson, 1956). Robinson (1956) was also the first to notice that the mesial roots of the M_1 in *P. robustus* exhibited a longitudinal depression (or gutter) on the mesial face of the root ending in a bifid or double apex of the root. In cross-section this is called a dumbbell-shaped root (see Fig. 1), and it has also been observed in the mesial roots of M_1 and M_2 of other early hominins, such as *Australopithecus afarensis*, *P. boisei*, *H. habilis*, and *H. rudolfensis* (Ward et al., 1982; Kullmer et al., 2011). Although there is some overlap in the extent of this mesiodistal root constriction in earlier hominins, the roots of later *Homo* (i.e., *H. erectus* and *H. sapiens*) appear to be more circular, without a constriction (Robinson, 1956; Kullmer et al., 2011).

Bifurcation height in the molars (i.e., the point where the root cervix splits into the mesial and distal root branches; see Fig. 1) can vary considerably within and between species. Following observations by Gorjanovic-Kramberger (1907, 1908) and Adloff (1907) on the molar roots of *H. neanderthalensis* from Krapina, Keith (1913) introduced the term ‘taurodontism’ to describe the

enlargement of the cervix and underlying pulp chamber at the expense of length of the root branches. Based on the varying degree of the apical displacement of the floor of the pulp chamber, molars have been classified into cyno-, hypo-, meso- and hypertaurodont forms using the so called taurodont index (Keene, 1966; Constant and Grine, 2001). While the anthropological and clinical dental assessment of taurodontism has traditionally been done using 2D lateral radiographs, Kupczik and Hublin (2010) used 3D surface models of mandibular molars and quantified the relative proportion of the volume of the root cervix and root branches, expressed as the volumetric bifurcation index. These authors found that hypertaurodont M_2 and M_3 with completely fused roots containing a single enlarged pulp cavity were common in *H. neanderthalensis*; in contrast, Kupczik and Hublin (2010) found no hypertaurodont molar roots in their sample of Late Pleistocene and recent *H. sapiens*. The pulp chamber and root canals house the dental pulp, blood vessels and nerves. The pulp tissue contains, among other things, odontoblasts, which deposit dentine at the periphery of the chamber during tooth development and in response to applied stimuli such as caries, trauma and wear (Berkovitz et al., 2002). It has been suggested that large pulp cavities of *H. neanderthalensis* may be an adaptation to a high-attrition dietary regimen because it allows for the deposition of secondary and tertiary dentine on the pulp walls following the loss of enamel and coronal dentine and thus prolongs tooth longevity (Blumberg et al., 1971; Constant and Grine, 2001; Kupczik and Hublin, 2010; Benazzi et al., 2015).

Aim of the study

By using the morphology of the mandibular molar roots, this study aims to shed further light on the taxonomic status of *H. naledi* compared to other Plio-Pleistocene fossil hominins from Africa and western Eurasia. Given the generally plesiomorphic signal of the dentition (Berger et al., 2015; Hawks et al., 2017) and similarities in mandibular shape (see Schroeder et al., 2017), we expect that

H. naledi will be more similar in root form to early *Homo* than to *H. sapiens* and *H. neanderthalensis*, with which it overlaps in time.

Materials and methods

Sample

A total of 183 mandibular first, second and third molars of three fossil hominin genera (*Australopithecus*, *Paranthropus* and *Homo*) were selected for this study (Table 1, Supplementary Online Material [SOM] Table S1). The specimens derive from collections housed at the following institutions: University of Witwatersrand, Johannesburg, South Africa; Ditsong National Museum of Natural History, Pretoria, South Africa and Iziko South African Museum, Cape Town, South Africa; National Museums of Kenya, Nairobi, Kenya; Sackler School of Medicine, Tel Aviv University, Tel Aviv, Israel; Institut National des Sciences de l'Archéologie et du Patrimoine, Rabat, Morocco; Geologisch-Paläontologisches Institut der Universität Heidelberg, Heidelberg, Germany; and the National Museum, Belgrade, Serbia. The *H. naledi* sample consisted of 13 mandibular molars belonging to six individuals from the Dinaledi Chamber of the Rising Star Cave in South Africa. The comparative *Homo* sample includes *H. habilis* and *H. erectus* (Kenya), *H. rudolfensis* (Malawi), *H. heidelbergensis* (Mauer and Balanica), *H. neanderthalensis* (various Eurasian sites), Pleistocene *H. sapiens* (also known as early anatomically modern humans) from Morocco (Dar es-Soltan, El Harhoura, and Irhoud), South Africa (Die Kelders and Equus Cave) and Israel (Qafzeh), as well as *Homo* sp. indet. from Kenya (Koobi Fora) and South Africa (Swartkrans and Cave of Hearths), respectively. Although KNM-ER 1805 has been assigned to *H. habilis* (Wood, 1991), SK 15 from Swartkrans Member 2 to *H. erectus* (Grine, 2005; Ungar et al., 2006), and Cave of Hearths to *H. sapiens rhodesiensis* (Tobias, 1971), there does not seem to be a

consensus on the taxonomic status of these specimens and we therefore took a more conservative approach by not assigning these fossils to any species. The same applies to SK 45 from Member 1 of Swartkrans, which resembles *H. habilis* more than it does *H. erectus* according to Grine (2005). In addition, with the exception of Amud 1 and Tabun C2, we used previously published data for *H. heidelbergensis* (see Skinner et al., 2016), *H. neanderthalensis*, and recent *H. sapiens* for comparison (see Kupczik and Hublin, 2010).

Microcomputed tomography imaging and image processing

The *H. naledi* dental remains were scanned on Nikon Metrology XTH 225/320 microtomography (microCT) scanner housed at the University of the Witwatersrand. The remaining fossil hominin mandibles, with the exception of the Equus Cave (EQ H-71/33) and Die Kelders Cave (SAM AP 6242) specimens, were scanned using a BIR ACTIS 225/300 high-resolution industrial microCT system or a SkyScan 1172 microtomographic scanner of the Max Planck Institute for Evolutionary Anthropology, Leipzig, Germany. The isometric voxel size ranged between 0.03 and 0.09 mm. EQ H-71/33 was scanned at ID 19 of the European Synchrotron Radiation Facility (Grenoble, France) with a voxel size of 0.03 mm, while SAM AP 6242 was scanned on a ScanCo 20 microCT system (Department of Biomedical Engineering, Stony Brook University, NY, USA) with a voxel size of 0.016 mm. All resulting CT images were filtered using a three-dimensional median filter (kernel size of 1) followed by a mean of least variance filter (kernel size of 1) following Kupczik and Hublin (2010). The filtering results in more homogenous dental tissue classes (enamel, dentine, pulp, bone) and allocates pixels with intermediate gray-scale values at tissue interfaces (e.g., enamel-dentine, dentine-pulp) to the appropriate tissue (Wollny et al., 2013). Each filtered dataset was imported into Avizo 9.1 (ThermoFisher Scientific™, Waltham, MA, USA) and, where possible, the enamel, dentine, and pulp were segmented using a combination

of semiautomatic thresholding and manual editing of the images. Some fossil specimens did not allow for a separation of the enamel from the coronal dentine, due to low contrast, and were thus segmented as one tissue material (i.e., dentine). After segmentation, triangulated surface models were generated using the constrained smoothing algorithm in Avizo. Subsequently, each molar model was virtually bisected into its anatomical crown and root parts by using a best-fit plane defined by up to 20 equally spaced points along the cementoenamel junction in Avizo. An additional plane parallel to this cervical plane was placed through the center of the interradicular surface (the bifurcational plane) to divide the roots into the root cervix and root branch (Fig. 1).

Tooth root morphometric analysis and statistical analysis

Observed variations in tooth root and pulp cavity morphology were described and visually shown through screenshots of the 3D molar models. The following terminology was used for describing variation in pulp morphology (Fig. 1): 1) pulp chamber = situated inside the crown and root cervix and houses nerves and blood vessels; 2) mesial root canal = thin, circular structure in the mesial roots extending from the base of the pulp chamber into the root branch; the inferior alveolar nerve and blood vessels enter through a single or double opening in the apex ; 3) distal root canal = elliptical or buccolingually flat conduit in the distal roots usually with a single foramen at the apex.

Furthermore, the following variables were quantified from the sectioned molar models (Fig. 1): root length (RL, in mm), cervical plane area (CPA, in mm^2), root surface area (RSA, in mm^2), total root volume (RV), root cervix volume (V_{cervix}) and root branch volume (V_{branch}), all in mm^3. To quantify the level of bifurcation, we computed a volumetric bifurcation index (VBI, in %) following Kupczik and Hublin (2010): $V_{cervix} / (V_{cervix} + V_{branch}) \times 100$. Corresponding with the classification scheme of Keene (1966) a value of 0–24.9% denotes a cynotaurodont molar, a value of 25–49.9% a hypotaurodont molar, a value 50–74.9% a mesotaurodont molar, and a value of 75–100% a

hypertaurodont molar. Bivariate associations between CPA and both RSA and RV were investigated using Pearson's correlation coefficient and ordinary least squares regression. A principal component analysis (PCA) using RL, CPA, V_{cervix}, and V_{branch} was conducted to compare tooth root morphology of *H. naledi* to the other fossil hominins in bivariate space. Moreover, a non-parametric multivariate analysis of variance (PERMANOVA) with pairwise PERMANOVAs between all pairs of taxonomic groups as a post hoc test was used to test for significant differences. All statistical analyses were performed in PAST v. 3.20 (Hammer et al., 2001).

Results

Comparative molar root and pulpal morphology

Lateral and apical views of the mandibular molar roots of the fossil hominins are presented in Figures 2 and 3, respectively. Detailed descriptions of the root and pulp morphology of each of the fossil specimens investigated here are presented in SOM S1 and illustrated in SOM Figs. 1–5. With the notable exception of the M_2 of U.W. 101-001 (*H. naledi*), Mauer, Irhoud 11, Qafzeh 9, and Qafzeh 25 (also the M_3), all fossil hominins have mandibular molars with well-separated, blade-like mesial and distal roots when viewed laterally (Fig. 2, SOM Figs. S1–S5). It is noteworthy that in *H. naledi* the distal roots of the M_3 are buccally offset relative to the mesial roots when viewed apically (Fig. 3). The deflection of the distalmost root is also observed in *Homo* sp. from Swartkrans (SK 15) and in *P. robustus* (Fig. 3; SOM Fig. S5). Moreover, in the *H. naledi* specimens U.W. 101-001, 361, 516 and 1261 the mesial and distal root apices of the M_3 show a depression on the buccal (U.W. 101-361 and 1261) or lingual (U.W. 101-001 and 516) aspect, which appears to be related to the inferior alveolar canal (Fig. 2; SOM Fig. S1). This feature is not observed in any of the other hominins. In all hominins, the mesial roots generally have bifid root apices, which correspond with

two separated root canals inside the root, while most of the distal roots house a single buccolingually expanded root canal (Fig. 4; SOM Figs. S1–S5). In cross section, the mesial roots have a figure-of-eight shape, whereas the distal roots are comma-shaped (Figs. 1 and 3). Unlike in the South African and Eurasian Pleistocene *H. sapiens*, where the root apices taper, in *H. naledi* the mesial root tips are set apart mesiodistally (SOM Figs. S1 and S4). The pulp chambers of the *H. naledi* molars are of low height in coronal-apical direction, similar to those of *H. rudolfensis*, *H. sapiens* (Irhoud 11), *Homo* sp. from Swartkrans, *A. africanus*, *P. boisei* and *P. robustus* (Fig. 4; SOM Figs. S1, S2, and S5). These are unlike the tall pulp chambers of *H. erectus*, *H. heidelbergensis*, *H. neanderthalensis* and *H. sapiens* (except Irhoud 11; Fig. 4; SOM Figs. S2–S4).

Molar root metrics and root volumetric proportions

Summary statistics are presented in Table 2 (individual specimen values are given in SOM Table S1). Overall, *H. naledi* root volumes fall within the same range as *A. africanus*, *H. neanderthalensis*, Pleistocene *H. sapiens*, and *Homo* sp. (Koobi Fora and Swartkrans), but are markedly smaller than those of *P. boisei*, *P. robustus*, *H. rudolfensis*, *H. habilis*, *H. erectus*, and *H. heidelbergensis*. In *H. naledi*, the M_2 has the largest root volume followed by the M_3 and M_1 (Fig. 5). Similar metameric variation is found in *A. africanus*, *P. robustus*, and *Homo* sp. from Swartkrans, while late *Homo* (*H. erectus*, *H. heidelbergensis*, *H. neanderthalensis*, and *H. sapiens*) tend to have larger M_1 than M_3 roots. *Paranthropus boisei* is the only hominin where the root metameric variation is $M_3 > M_2 > M_1$ (Fig. 5).

Homo naledi molar roots have volumetric bifurcation values of ≤43% throughout all molar positions (with the exception of the M_3 of U.W. 101-1142, which has a value of 53%; SOM Table S1) and are thus classified as hypotaurodont (Table 2; Fig. 6). While the M_2 roots of the *P. boisei* specimen KNM-ER 3230 are cynotaurodont (17%), hypotaurodont molars are also found in the two

Paranthropus species (in particular at M_1) and in the *Homo* sp. specimens from Koobi Fora (KNM-ER 1805: M_2 = 37%, M_3 = 30%) and Swartkrans (SK 45: M_1 = 30%, M_2 = 34%), but not SK 15 (M_1 = 46%, M_2 = 46%, M_3 = 56%) and Cave of Hearths (M_1 = 48%; SOM Table S1). The molar roots of *H. habilis* and *H. erectus* are also hypotaurodont, while *H. rudolfensis* is mesotaurodont (Fig. 6; SOM Table S1). The hypotaurodont molars of *H. naledi* are contrasted by the meso- and hypertaurodont molar roots of late *Homo* species (specifically Pleistocene *H. sapiens* from Equus Cave and Qafzeh) with values ≥ 50%, in particular at M_2 and M_3 (Table 2; SOM Table S1; Fig. 6).

Bivariate associations

Cervical plane area (CPA) is highly correlated with both RV and RSA in all three molar positions (Table 3; Fig. 7; SOM Figs. S6 and S7). Relative to CPA, *H. erectus*, *H. heidelbergensis*, *H. neanderthalensis*, *Homo* sp. KNM-ER1805 (M_3 only) and *P. boisei* (M_2 and M_3 only) have relatively large root volumes, as indicated by the positive regression residuals (Fig. 7; SOM Fig. S6). Likewise, *H. naledi* M_1 and M_2 have relatively large RV for a given CPA, while the M_3 has a RV as expected for its CPA (Fig. 7; SOM Fig. S6). In contrast, *A. africanus*, *H. habilis*, *H. rudolfensis*, *Homo* sp. from Swartkrans, and *H. sapiens* (both Pleistocene and recent) have relatively small molar RV for a given CPA (Fig. 7; SOM Fig. S6, negative residuals). The same relationship is largely observed when RSA is considered (SOM Fig. S7).

Principal components analysis and PERMANOVA

Principal component loadings reveal that, for all three molar positions, RL, CPA and V_{branch} contribute most to the first component (PC1), whereas V_{cervix} contributes most to the second (PC2; Table 4). *Homo naledi* forms a separated cluster from the remainder of the sample in all three molar

positions (Fig. 8). Along PC1, *H. naledi* is most comparable to *H. sapiens* (Pleistocene and modern) and *H. neanderthalensis*, which reflects its small root size. Along PC2, *H. naledi* overlaps with *P. boisei* and *P. robustus*, which reflects the hypotaurodont root morphology captured in the univariate analysis above. *Australopithecus africanus* overlaps with some Pleistocene *H. sapiens*, *H. neanderthalensis*, and *P. robustus*. Perhaps with the exception of the M_1 of SK 15, which is similar to that of the Pleistocene *H. sapiens* from Temara, the molar roots of the *Homo* sp. fossils from Swartkrans and Koobi Fora are closer to *H. naledi* than to any other African *Homo* (Fig. 8; SOM Fig. S8). *Homo erectus* (in particular the M_1) also forms a separate cluster from the rest of the fossil hominins and does not bear much resemblance with the *H. naledi* hypodigm.

The PERMANOVAs revealed significant differences across the taxonomic groups at all three molar positions (M_1: $F = 16.89$; M_2: $F = 12.86$; M_3: $F = 10.65$; all $p < 0.0001$). The pairwise PERMANOVAs as a post hoc test between all pairs of groups showed some significant differences (at $p < 0.05$) for M_1 (SOM Table S2): between *H. naledi* and recent *H. sapiens*; between recent *H. sapiens* and *H. neanderthalensis*, Pleistocene *H. sapiens* and *P. robustus*; and between *H. neanderthalensis* and *P. boisei*. For the M_2, pairwise significant differences were found between *P. robustus* and *H. neanderthalensis*, and between *P. robustus* and both Pleistocene and recent *H. sapiens* (SOM Table S3). No significant pairwise difference was found in M_3 (SOM Table S4).

Discussion

When root size and proportion as well as metameric variation collectively are taken into account, *H. naledi* shows a mix of ancestral (early *Homo*, *A. africanus*, *P. boisei*, and *P. robustus*) and derived (late *Homo*) features (Figs. 4–8). *Homo naledi* has markedly smaller roots than those of eastern African *H. rudolfensis*, *H. habilis*, and *H. erectus* but shares similar root and pulp (*H.*

rudolfensis only) proportions with these taxa (Table 2; Figs. 4–8). In contrast, *H. naledi* has molar root sizes comparable to Pleistocene *H. sapiens* but, unlike these, has different root proportions (i.e., they are less taurodont with a narrow pulp chamber in *H. naledi*; see Table 2; Figs. 4–6). Interestingly, the three *Homo* fossils from Swartkrans (SK 45 from Member 1 and SK 15 from Member 2) and Koobi Fora (KNM-ER 1805), which have been assigned by some to *H. erectus*, *Homo* sp. indet., and *H. habilis*, respectively (Broom and Robinson, 1949, 1950; Robinson, 1961; Wood, 1991; Grine, 2005; Ungar et al., 2006; Grine et al., 2009; Moggi-Cecchi et al., 2010), bear the largest resemblance in overall appearance (i.e., root size, proportion and metameric variation) with the *H. naledi* hypodigm (see Figs. 3–6 and 8). Both *H. naledi* and *Homo* sp. SK 15 exhibit distal M_3 roots which are buccally offset relative to the mesial roots; a feature they share with *P. robustus* (Fig. 3). In *H. naledi* this root deflection in conjunction with the observed depression on the buccal aspect of both the mesial and distal M_3 roots appears to be related to the passage of the inferior alveolar canal running parallel to the M_3 root rather than beneath it as can be seen in *A. africanus* Stw 498c (Fig. 3; SOM Figs. S1 and S5).

Homo naledi and *Homo* sp. SK 15 are also similar in terms of the corono-apical constriction of the pulp chamber, which is also found in African early hominins but not in late *Homo* with the exception of *H. sapiens* from Irhoud (Fig. 3). Meso- and hypertaurodont molars are the result of enlarged pulp cavities and these are particularly common in *H. heidelbergensis* and *H. neanderthalensis* (Kupczik and Hublin, 2010; Skinner et al., 2016). This trait is suggested to be an adaptation to counter marked occlusal wear because a large pulp chamber may allow for the deposition of secondary dentine on the walls of the pulp (Blumberg et al., 1971; Constant and Grine, 2001), although the physiological mechanism may be different across species. For example, it was found that in worn molars of Middle Pleistocene *H. neanderthalensis* the pulp horns and walls were obliterated with secondary deposition, while in hypotaurodont molars of late Pleistocene

H. sapiens from North Africa dentine was predominantly deposited on the roof and floor in the center of the pulp chamber (Kupczik and Hublin, 2010). Although some of the M_1 and M_2 of *H. naledi* are heavily worn with dentine exposure (e.g., U.W. 101-001 and U.W. 101-361; see SOM Fig. S1), there is no indication of an obliterated pulp chamber or root canal.

Moreover, while SK 15 has relatively smaller roots when scaled to cervical plane area compared to both *H. naledi* and SK 45 (root surface area only; see Fig. 7; SOM Fig. S7), it shares with *H. naledi* the same root size gradient ($M_2 > M_3 > M_1$; see Fig. 5). This gradient is also found in *A. africanus*, *P. robustus*, and *P. boisei* specimen KNM-ER 15930 (KNM-ER 729 has $M_2 = M_3 > M_1$) but not in any of the other *Homo* fossils, including *H. erectus* and Pleistocene *H. sapiens* from North Africa and the Near East ($M_2 > M_1 > M_3$; Fig. 5)[1]. Since the *H. erectus*/late *Homo* root volume sequence is also found in two African great apes, *Pan troglodytes* and *Gorilla gorilla* (Kupczik, 2003), this may in fact constitute the plesiomorphic state; thus, it is derived in *A. africanus*, *P. robustus*, *P. boisei* and *H. naledi*. In contrast, cervical plane area follows the previously reported crown area gradient of $M_3 > M_2 > M_1$ (Table 2), which is also present in *H. habilis* but not in *H. erectus* or late *Homo* (see Berger et al., 2015; Evans et al., 2016; Hawks et al., 2017).

It has recently been suggested that the Middle Pleistocene Cave of Hearths mandible, which has been assigned to *H. sapiens rhodesiensis* (Tobias, 1971), could belong to *H. naledi* (Berger et al., 2017). However, this is unlikely given that the Cave of Hearths mandible differs from the latter in several dental morphological features including occlusal topography of the M_2 (Berthaume et al., 2018), overall premolar and molar crown morphology (L.K.D., pers. obs.) and, as shown here, M_1 root morphology (SOM Figs. S2, S3, and S7). In fact, both external root form (e.g., the tapering

[1] It appears that KNM-ER 1805 has the same root size sequence as *H. naledi* and SK 15 (Fig. 2); however, we did not report the M_1 root metrics here because the tooth is partially broken at the cervix.

mesial M_1 root) and the morphology of the root canals of the Cave of Hearths specimen resemble those of Middle and Upper Pleistocene *H. sapiens* from North Africa (Irhoud 11), South Africa (Die Kelders, Equus Cave) and Qafzeh (see Kupczik and Hublin, 2010: Fig. S1; SOM Figs. S2 and S4). These results suggest that this specimen is most closely affiliated with samples of fossil *H. sapiens* (or potentially *H. rhodesiensis* if the early part of the *H. sapiens* lineage is distinguished at the species rank). Other notable African Middle Pleistocene *Homo* fossils, such as the ca. 700 ka Tighenif 2 from Algeria (Geraads et al., 1986), differ in mandibular molar root volume and metameric variation from *H. naledi* and rather fall within the upper range of the Aterian *H. sapiens* (Kupczik and Hublin, 2010; Zanolli and Mazurier, 2013). Based on the data in Zanolli and Mazurier (2013: Table 1), the sequence of root volumes of Tighenif 2 follows the $M_2 > M_1 > M_3$ pattern seen in late *Homo* (M_1 = 951.07 mm^3, M_2 = 1051.29 mm^3, M_3 = 773.39 mm^3). Although there are no root metric data available for the mandibular teeth of *H. erectus* from Dmanisi, at least the mandible D211 is distinct from the *H. naledi* lower molar roots inasmuch as the M_1 appears to be larger than the M_2 (see also Hawks et al., 2017). Moreover, while the M_1 has clearly separated roots, the M_2 and M_3 roots of D211 appear to be fused or hypertaurodont (see Margvelashvili et al., 2013: their Fig. 2). In contrast, the molars of the mandibles D2735 and D2600 have separated mesial and distal roots. It is also interesting to note that, on visual inspection of the reconstructions of the Dmanisi teeth (see Margvelashvili et al., 2013), the large mandible D2600 has long and distally curved molar roots with a high bifurcation, while the smaller D2735 (comparable in size with D211) has concomitantly shorter and straight molar roots. Unlike in the Dmanisi sample, the differences in molar root morphology within the *H. naledi* sample investigated here do not appear to be as marked.

Conclusions

The present findings on mandibular molar root morphology concur with those of previous studies that *H. naledi* is characterized by a mosaic of ancestral and derived cranial and postcranial features. Thus, while absolute molar root size aligns *H. naledi* with late *Homo*, including Middle and Late Pleistocene *H. sapiens* from South Africa (Cave of Hearths, Die Kelders, Equus Cave) and North Africa (Irhoud, Temara, Dar-Es-Soltan), this species shares hypotaurodont roots and a root size gradient with early *Homo* and *Paranthropus*. The latter root traits likely constitute the ancestral condition and are thus symplesiomorphies between *H. naledi* and these earlier hominins. Although this study did not necessarily aim to resolve the phylogenetic relationships of *H. naledi* per se, the present findings shed some light of the possible evolutionary trends of hominins in eastern and southern Africa. If specimens like Cave of Hearth are indeed much older than our sample of *H. naledi*, it points to an ancient origin for the modern human molar root pattern and suggests that it is unlikely that modern humans derive substantial ancestry from *H. naledi*. Since molar root form has the advantage of being conservative in its phenotypic expression and roots are often better preserved than crowns in the fossil record, molar root morphological characters may prove useful in future studies on the evolutionary relationships in hominins in general.

Acknowledgements

For support of the research of the analysis of the *H. naledi* dental material we thank Lee Berger and John Hawks. For access to specimens and CT scans we thank Heidi Fourie and Stephany Potze, and the Ditsong National Museum of Natural History (Pretoria, South Africa); Bernard Zipfel, Sifelani Jura, and the University of Witwatersrand (Johannesburg, South Africa); Emma Mbua and the National Museums of Kenya, Nairobi, Kenya; Fred Grine and Stefan Judex (Stony Brook

University, NY, USA); Paul Tafforeau and the European Synchrotron Radiation Facility (Grenoble, France); Yoel Rak and Alon Barash and Tel Aviv University; Friedemann Schrenk and Ottmar Kullmer and the Senckenberg Research Institute (Frankfurt, Germany); Mirjana Roksandic (The University of Winnipeg, Canada); and Jean-Jacques Hublin (Max Planck Institute for Evolutionary Anthropology, Leipzig, Germany). Tomographic scans of some specimens were produced through a collaborative project between the Department of Human Evolution, Max Planck Institute for Evolutionary Anthropology and the Evolutionary Studies Institute and Centre for Excellence in Paleo-Sciences, Johannesburg, South Africa. For scanning and technical assistance we thank Kudakwashe Jakata, Tracy Kivell, Collin Moore, David Plotzki, Patrick Schoenfeld, Fred Spoor, Adam Sylvester, Heiko Temming, Francis Thackeray and Andreas Winzer. For discussions and comments on this project we are grateful to Adeline Le Cabec. We are very grateful to the Editor, (David Alba), Associate Editor (Clément Zanolli) and three anonymous reviewers for their constructive comments to improve this manuscript. This research was supported by a workshop grant (to L.K.D. and M.M.S.) from the Wenner-Gren Foundation and the Max Planck Society (to K.K. and M.M.S.). Financial support for L.K.D. was provided by a Connor Family Faculty Fellowship and the Office of Research and Development at the University of Arkansas.

References

Abbott, S.A., 1984. A comparative study of tooth root morphology in the great apes, modern man and early hominids. Ph.D. Dissertation, University of London.

Adloff, P., 1907. Die Zähne des *Homo primigenius* von Krapina. Anatomischer Anzeiger 31, 273-282.

Benazzi, S., Nguyen, H.N., Kullmer, O., Hublin, J.-J., 2015. Exploring the biomechanics of taurodontism. Journal of Anatomy 226, 180-188.

Berger, L.R., Hawks, J., de Ruiter, D.J., Churchill, S.E., Schmid, P., Delezene, L.K., Kivell, T.L.,

Garvin, H.M., Williams, S.A., DeSilva, J.M., Skinner, M.M., Musiba, C.M., Cameron, N., Holliday, T.W., Harcourt-Smith, W., Ackermann, R.R., Bastir, M., Bogin, B., Bolter, D., Brophy, J., Cofran, Z.D., Congdon, K.A., Deane, A.S., Dembo, M., Drapeau, M., Elliott, M.C., Feuerriegel, E.M., Garcia-Martinez, D., Green, D.J., Gurtov, A., Irish, J.D., Kruger, A., Laird, M.F., Marchi, D., Meyer, M.R., Nalla, S., Negash, E.W., Orr, C.M., Radovcic, D., Schroeder, L., Scott, J.E., Throckmorton, Z., Tocheri, M.W., VanSickle, C., Walker, C.S., Wei, P., Zipfel, B., 2015. *Homo naledi*, a new species of the genus *Homo* from the Dinaledi Chamber, South Africa. eLife 4, e09560.

Berger, L.R., Hawks, J., Dirks, P.H.G.M., Elliott, M., Roberts, E.M., 2017. *Homo naledi* and Pleistocene hominin evolution in subequatorial Africa. eLife 6, e24234.

Berkovitz, B.K., Holland, G.R., Moxham, B.J., 2002. Oral Anatomy, Histology and Embryology, 1st ed. Mosby, St. Louis.

Bermúdez de Castro, J.M., Martinón-Torres, M., Sier, M.J., Martín-Francés, L., 2014. On the Variability of the Dmanisi Mandibles. PLoS One 9, e88212.

Bermúdez de Castro, J.M., Rosas, A., Nicolás, M.E., 1999. Dental remains from Atapuerca-TD6 (Gran Dolina site, Burgos, Spain). Journal of Human Evolution 37, 523-566.

Berthaume, M.A., Delezene, L.K., Kupczik, K., 2018. Dental topography and the diet of *Homo naledi*. Journal of Human Evolution 118, 14-26.

Blumberg, J.E., Hylander, W.L., Goepp, R.A., 1971. Taurodontism: a biometric study. American Journal of Physical Anthropology 34, 243-255.

Broom, R., Robinson, J.T., 1949. A new type of fossil man. Nature 164, 322.

Broom, R., Robinson, J.T., 1950. Man contemporaneous with the Swartkrans ape-man. American Journal of Physical Anthropology 8, 151-156.

Constant, D., Grine, F., 2001. A review of taurodontism with new data on indigenous southern African populations. Archives of Oral Biology 46, 1021-1029.

Constantino, P.J., Lee, J.J.-W., Chai, H., Zipfel, B., Ziscovici, C., Lawn, B.R., Lucas, P.W., 2010. Tooth chipping can reveal the diet and bite forces of fossil hominins. Biology Letters 6, 826-829.

Dembo, M., Radovčić, D., Garvin, H.M., Laird, M.F., Schroeder, L., Scott, J.E., Brophy, J., Ackermann, R.R., Musiba, C.M., de Ruiter, D.J., Mooers, A.Ø., Collard, M., 2016. The evolutionary relationships and age of *Homo naledi*: An assessment using dated Bayesian phylogenetic methods. Journal of Human Evolution 97, 17-26.

Demes, B., Creel, N., 1988. Bite force, diet, and cranial morphology of fossil hominids. Journal of Human Evolution 17, 657-670.

Dirks, P.H.G.M., Roberts, E.M., Hilbert-Wolf, H., Kramers, J.D., Hawks, J., Dosseto, A., Duval, M., Elliott, M., Evans, M., Grün, R., Hellstrom, J., Herries, A.I.R., Joannes-Boyau, R., Makhubela, T.V., Placzek, C.J., Robbins, J., Spandler, C., Wiersma, J., Woodhead, J., Berger, L.R., 2017. The age of *Homo naledi* and associated sediments in the Rising Star Cave, South Africa. eLife 6, e24231.

Emonet, E.G., Andossa, L., Taisso Mackaye, H., Brunet, M., 2014. Subocclusal dental morphology of *Sahelanthropus tchadensis* and the evolution of teeth in hominins. American Journal of Physical Anthropology 153, 116-123.

Emonet, E.G., Tafforeau, P., Chaimanee, Y., Guy, F., de Bonis, L., Koufos, G., Jaeger, J.J., 2012. Three-dimensional analysis of mandibular dental root morphology in hominoids. Journal of Human Evolution 62, 146-154.

Eng, C.M., Lieberman, D.E., Zink, K.D., Peters, M.A., 2013. Bite force and occlusal stress production in hominin evolution. American Journal of Physical Anthropology 151, 544-557.

Evans, A.R., Daly, E.S., Catlett, K.K., Paul, K.S., King, S.J., Skinner, M.M., Nesse, H.P., Hublin, J.-J., Townsend, G.C., Schwartz, G.T., Jernvall, J., 2016. A simple rule governs the evolution and development of hominin tooth size. Nature 530, 477.

Feuerriegel, E.M., Green, D.J., Walker, C.S., Schmid, P., Hawks, J., Berger, L.R., Churchill, S.E.,

2017. The upper limb of *Homo naledi*. Journal of Human Evolution 104, 155-173.

Garvin, H.M., Elliott, M.C., Delezene, L.K., Hawks, J., Churchill, S.E., Berger, L.R., Holliday, T.W., 2017. Body size, brain size, and sexual dimorphism in *Homo naledi* from the Dinaledi Chamber. Journal of Human Evolution 111, 119-138.

Geraads, D., Hublin, J.-J., Jaeger, J.-J., Tong, H., Sen, S., Toubeau, P., 1986. The Pleistocene hominid site of Ternifine, Algeria: new results on the environment, age, and human industries. Quaternary Research 25, 380-386.

Gorjanovic-Kramberger, D., 1907. Die Kronen und Wurzeln der Mahlzähne des *Homo primigenius* und ihre genetische Bedeutung. Anatomischer Anzeiger 31, 97-134.

Gorjanovic-Kramberger, D., 1908. Über prismatische Molarwurzeln rezenter und diluvialer Menschen. Anatomischer Anzeiger 32, 401-413.

Grabowski, M., Hatala, K.G., Jungers, W.L., Richmond, B.G., 2015. Body mass estimates of hominin fossils and the evolution of human body size. Journal of Human Evolution 85, 75-93.

Grine, F.E., 2005. Early Homo at Swartkrans, South Africa: a review of the evidence and an evaluation of recently proposed morphs. South African Journal of Science 101, 43-52.

Grine, F.E., Smith, H.F., Heesy, C.P., Smith, E.J., 2009. Phenetic affinities of Plio-Pleistocene Homo fossils from South Africa: molar cusp proportions, in: Grine, F.E., Fleagle, J.G., Leakey, R.E.F. (Eds.), The First Humans–Origin and Early Evolution of the Genus *Homo*. Springer, Dordrecht, pp. 49-62.

Hammer, Ø., Harper, D.A.T., Ryan, P.D., 2001. PAST: Paleontological statistics software package for education and data analysis. Palaeontologia Electronica 4, 4.

Harcourt-Smith, W.E.H., Throckmorton, Z., Congdon, K.A., Zipfel, B., Deane, A.S., Drapeau, M.S.M., Churchill, S.E., Berger, L.R., DeSilva, J.M., 2015. The foot of *Homo naledi*. Nature Communications 6, 8432.

Hawks, J., Elliott, M., Schmid, P., Churchill, S.E., Ruiter, D.J.d., Roberts, E.M., Hilbert-Wolf, H.,

Garvin, H.M., Williams, S.A., Delezene, L.K., Feuerriegel, E.M., Randolph-Quinney, P., Kivell, T.L., Laird, M.F., Tawane, G., DeSilva, J.M., Bailey, S.E., Brophy, J.K., Meyer, M.R., Skinner, M.M., Tocheri, M.W., VanSickle, C., Walker, C.S., Campbell, T.L., Kuhn, B., Kruger, A., Tucker, S., Gurtov, A., Hlophe, N., Hunter, R., Morris, H., Peixotto, B., Ramalepa, M., Rooyen, D.v., Tsikoane, M., Boshoff, P., Dirks, P.H.G.M., Berger, L.R., 2017. New fossil remains of *Homo naledi* from the Lesedi Chamber, South Africa. eLife 6, e24232.

Irish, J.D., Bailey, S.E., Guatelli-Steinberg, D., Delezene, L.K., Berger, L.R., 2018. Ancient teeth, phenetic affinities, and African hominins: Another look at where *Homo naledi* fits in. Journal of Human Evolution 122, 108-123.

Keene, H., 1966. A morphologic and biometric study of taurodontism in a contemporary population. American Journal of Physical Anthropology 25, 208-209.

Keith, A., 1913. Problems relating to the teeth of the earlier forms of prehistorical man. Proceedings of the Royal Society of Medicine 6, 103-119.

Kivell, T.L., Deane, A.S., Tocheri, M.W., Orr, C.M., Schmid, P., Hawks, J., Berger, L.R., Churchill, S.E., 2015. The hand of *Homo naledi*. Nature Communications 6, 8431.

Kullmer, O., Sandrock, O., Kupczik, K., Frost, S.R., Volpato, V., Bromage, T.G., Schrenk, F., 2011. New primate remains from Mwenirondo, Chiwondo Beds in northern Malawi. Journal of Human Evolution 61, 617-623.

Kupczik, K., 2003. Tooth root morphology in primates and carnivores. Ph.D. Dissertation, University College London.

Kupczik, K., Dean, M.C., 2008. Comparative observations on the tooth root morphology of *Gigantopithecus blacki*. Journal of Human Evolution 54, 196-204.

Kupczik, K., Hublin, J.J., 2010. Mandibular molar root morphology in Neanderthals and Late Pleistocene and recent *Homo sapiens*. Journal of Human Evolution 59, 525-541.

Kupczik, K., Olejniczak, A.J., Skinner, M.M., Hublin, J.J., 2009. Molar crown and root size

relationship in anthropoid primates. Frontiers in Oral Biology 13, 16-22.

Kupczik, K., Spoor, F., Pommert, A., Dean, M.C., 2005. Premolar root number variation in hominoids: genetic polymorphism vs. functional significance. In: Żądzińska, E. (Ed.), Current Trends in Dental Morphology Research. University of Lodz Press, Lodz, pp 257-268.

Kupczik, K., Stynder, D.D., 2012. Tooth root morphology as an indicator for dietary specialization in carnivores (Mammalia: Carnivora). Biological Journal of the Linnean Society 105, 456-471.

Laird, M.F., Schroeder, L., Garvin, H.M., Scott, J.E., Dembo, M., Radovčić, D., Musiba, C.M., Ackermann, R.R., Schmid, P., Hawks, J., Berger, L.R., de Ruiter, D.J., 2017. The skull of *Homo naledi*. Journal of Human Evolution 104, 100-123.

Le Cabec, A., Gunz, P., Kupczik, K., Braga, J., Hublin, J.J., 2013. Anterior tooth root morphology and size in Neanderthals: taxonomic and functional implications. Journal of Human Evolution 64, 169-193.

Le Cabec, A., Skinner, M.M., Delezene, L.K., 2017. What can anterior tooth root morphometrics tell us about *Homo naledi*? Proceedings of the European Society for the Study of Human Evolution 6, 112.

Lucas, P., Constantino, P., Wood, B., Lawn, B., 2008. Dental enamel as a dietary indicator in mammals. BioEssays 30, 374-385.

Margvelashvili, A., Zollikofer, C.P.E., Lordkipanidze, D., Peltomäki, T., Ponce de León, M.S., 2013. Tooth wear and dentoalveolar remodeling are key factors of morphological variation in the Dmanisi mandibles. Proceedings of the National Academy of Sciences USA 110, 17278-17283.

Moggi-Cecchi, J., Menter, C., Boccone, S., Keyser, A., 2010. Early hominin dental remains from the Plio-Pleistocene site of Drimolen, South Africa. Journal of Human Evolution 58, 374-405.

Moore, N.C., Hublin, J.J., Skinner, M.M., 2015. Premolar root and canal variation in extant non-human hominoidea. American Journal of Physical Anthropology 158, 209-226.

Moore, N.C., Thackeray, J.F., Hublin, J.J., Skinner, M.M., 2016. Premolar root and canal variation

in South African Plio-Pleistocene specimens attributed to *Australopithecus africanus* and *Paranthropus robustus*. Journal of Human Evolution 93, 46-62.

Robinson, J.T., 1956. The Dentition of Australopithecinae. Transvaal Museum, Pretoria.

Robinson, J.T., 1961. The Australopithecines and their bearing on the origin of man and of stone tool-making. South African Journal of Science 57, 3-13.

Schroeder, L., Scott, J.E., Garvin, H.M., Laird, M.F., Dembo, M., Radovčić, D., Berger, L.R., de Ruiter, D.J., Ackermann, R.R., 2017. Skull diversity in the *Homo* lineage and the relative position of Homo naledi. Journal of Human Evolution 104, 124-135.

Scott, G.R., Turner Ii, C.G., Townsend, G.C., Martinón-Torres, M., 2018. The Anthropology of Modern Human Teeth: Dental Morphology and Its Variation in Recent and Fossil *Homo sapiens*, 2nd ed. Cambridge University Press, Cambridge.

Shields, E.D., 2005. Mandibular premolar and second molar root morphological variation in modern humans: What root number can tell us about tooth morphogenesis. American Journal of Physical Anthropology 128, 299-311.

Skinner, M.M., de Vries, D., Gunz, P., Kupczik, K., Klassen, R.P., Hublin, J.-J., Roksandic, M., 2016. A dental perspective on the taxonomic affinity of the Balanica mandible (BH-1). Journal of Human Evolution 93, 63-81.

Spencer, M.A., 1998. Force production in the primate masticatory system: electromyographic tests of biomechanical hypotheses. Journal of Human Evolution 34, 25-54.

Spencer, M.A., 2003. Tooth-root form and function in platyrrhine seed-eaters. American Journal of Physical Anthropology 122, 325-335.

Sperber, G., 1974. The morphology of the cheek teeth of early South African hominids. Ph.D. Dissertation, University of the Witwatersrand.

Tobias, P.V., 1971. Human skeletal remains from the cave of Hearths, Makapansgat, Northern Transvaal. American Journal of Physical Anthropology 34, 335-367.

Towle, I., Irish, J.D., De Groote, I., 2017. Behavioral inferences from the high levels of dental chipping in *Homo naledi*. American Journal of Physical Anthropology 164, 184-192.

Turner, C.G., 1971. Three-rooted mandibular first permanent molars and the question of American Indian Origins. American Journal of Physical Anthropology 34, 229-241.

Ungar, P.S., Berger, L.R., 2018. Brief communication: Dental microwear and diet of *Homo naledi*. American Journal of Physical Anthropology 166, 228-235.

Ungar, P.S., Grine, F.E., Teaford, M.F., El Zaatari, S., 2006. Dental microwear and diets of African early *Homo*. Journal of Human Evolution 50, 78-95.

VanSickle, C., Cofran, Z., García-Martínez, D., Williams, S.A., Churchill, S.E., Berger, L.R., Hawks, J., 2017. *Homo naledi* pelvic remains from the Dinaledi Chamber, South Africa. Journal of Human Evolution 125, 122-136.

Ward, S.C., Johanson, D.C., Coppens, Y., 1982. Subocclusal morphology and alveolar process relationships of hominid gnathic elements from the Hadar formation: 1974–1977 collections. American Journal of Physical Anthropology 57, 605-630.

Wollny, G., Kellman, P., Ledesma-Carbayo, M.-J., Skinner, M.M., Hublin, J.-J., Hierl, T., 2013. MIA - A free and open source software for gray scale medical image analysis. Source Code for Biology and Medicine 8, 20.

Wood, B.A., 1988. Are “robust” australopithecines a monophyletic group? In: Grine, F.E. (Ed.), Evolutionary History of the ‘‘Robust’’ Australopithecines. Aldine de Gruyter, New York, pp. 269–284.

Wood, B.A., 1991. Hominid Cranial Remains. Clarendon Press, Oxford.

Wood, B.A., Abbott, S.A., Uytterschaut, H., 1988. Analysis of the dental morphology of Plio-Pleistocene hominids. IV. Mandibular postcanine root morphology. Journal of Anatomy 156, 107-139.

Zanolli, C., Mazurier, A., 2013. Endostructural characterization of the *H. heidelbergensis* dental

remains from the early Middle Pleistocene site of Tighenif, Algeria. Comptes Rendus Palevol 12, 293-304.

Figure legends

Figure 1. Microtomography-based 3D-reconstructions of a modern human left M_2 (center) and pulp cavity morphology (left) in mesiolingual view. The tooth was virtually trisected into the crown, root cervix and root branch at the cervical plane and bifurcational plane, respectively (right). The area between the crown and the root cervix is the cervical plane area (CPA). Root length (RL) was measured at the mesial root as the projected distance between the cervical plane and the root tip. The cross-sections illustrate the shape of the mesial and distal root in the apical third of the root (bottom).

Figure 2. Microtomographic-based 3D reconstructions of mandibular molars in fossil hominins in buccal view: a) U.W. 101-1261 (right); the arrows indicate a depression in the apices of the mesial and distal roots of the M_3; b) SK 15 (right); c) Irhoud 11 (left); d) Amud 1 (left); e) HCRP-UR501 (right M_1 and M_2); f) KNM-ER 1802 (left M_1 and M_2); g) KNM-ER 1805 (left); h) KNM-ER 730 (left); i) STW 404 (left); j) SK 23 (left); k) KNM-ER 729 (right). M_1 is to the left of the molar row. Note that the right molar rows are horizontally flipped. m=mesial, l=lingual.

Figure 3. Microtomographic-based 3D reconstructions of mandibular molars in fossil hominins in apical view: a) U.W. 101-001 (right M_1–M_3); b) U.W.101-1261 (right M_1–M_3); c) U.W.101-1142 (right M_2–M_3); d) U.W.101-361 (left M_2–M_3); e) U.W.101-516 (left M_3); f) SK 15 (right M_1–M_3); g) KNM-ER 730 (left M_1–M_3); h) KNM-ER 1805 (left M_1–M_3); i) Irhoud 11 (left M_1–M_3); j) Qafzeh 2 (left M_1–M_3); k) EQ-H71-33 (left M_2–M_3); l) Mauer (right M_1–M_3); m) Amud 1 (left M_1–M_3); n) Stw 498c (left M_1–M_3); o) SK 23 (left M_1–M_3); p) KNM-ER 15930 (left M_1–M_3). Mesial is to the top and buccal to the right. The arrows indicate a buccally deflected distal M_3 root relative to

the mesial root. Note that the left molar rows are horizontally flipped. m=mesial, b=buccal.

Figure 4. Pulp chamber morphology of mandibular second molars in *H. naledi* compared to other hominin species in lateral view: a) *A. africanus* (Stw 498c), *P. robustus* (SK 1586), and *P. boisei* (KNM-ER 729) with low pulp chambers; b) species of *Homo* with low pulp chambers (left to right: HCRP-UR 501, SK 15, Irhoud 11, and UW101-1142); c) species of *Homo* with tall pulp chambers (left to right: KNM-ER 992, BH1, and Tabun II C2). All molars are aligned using the lower horizontal line marking the lower border of the pulp cavity. The upper line marks the upper border of the pulp cavity of *H. naledi*.

Figure 5. Box-and-whisker plot of mandibular molar root volume (in mm^3). The horizontal lines depict medians, the boxes indicate the lower and upper quartile, respectively, and the lower and upper whiskers show the lowest and highest value, respectively.

Figure 6. Relative proportions of cervical and root branch volumes (scaled to 100%) in Plio-Pleistocene fossil hominins

Figure 7. Bivariate plot of molar root area against cervical plane area in a) M_1, b) M_2, and c) M_3. Ordinary least square regression line (solid) and 95% confidence intervals (dashed) are shown.

Figure 8. Bivariate plots of second vs. first principal components (PC2 vs. PC1) using four root metrics: a) M_1; b) M_2; c) M_3. Abbreviations: Aa = *Australopithecus africanus*; Hb = *Homo heidelbergensis*; He = *Homo erectus*; Hh = *Homo habilis*; Hn = *Homo neanderthalensis*; Hnl =

Homo naledi; Hr = *Homo rudolfensis*; Hs = recent *Homo sapiens*; HsP = Pleistocene *Homo sapiens*; Pb = *Paranthropus boisei*; Pr = *Paranthropus robustus*.

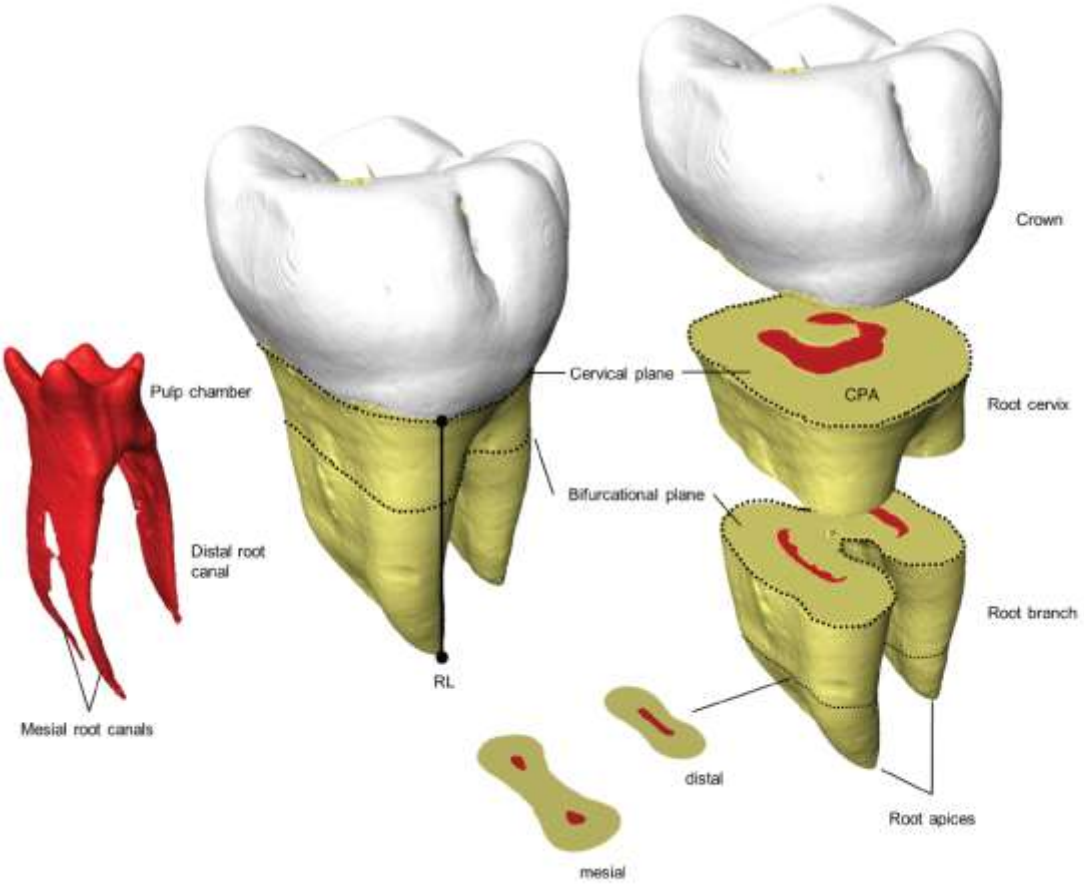

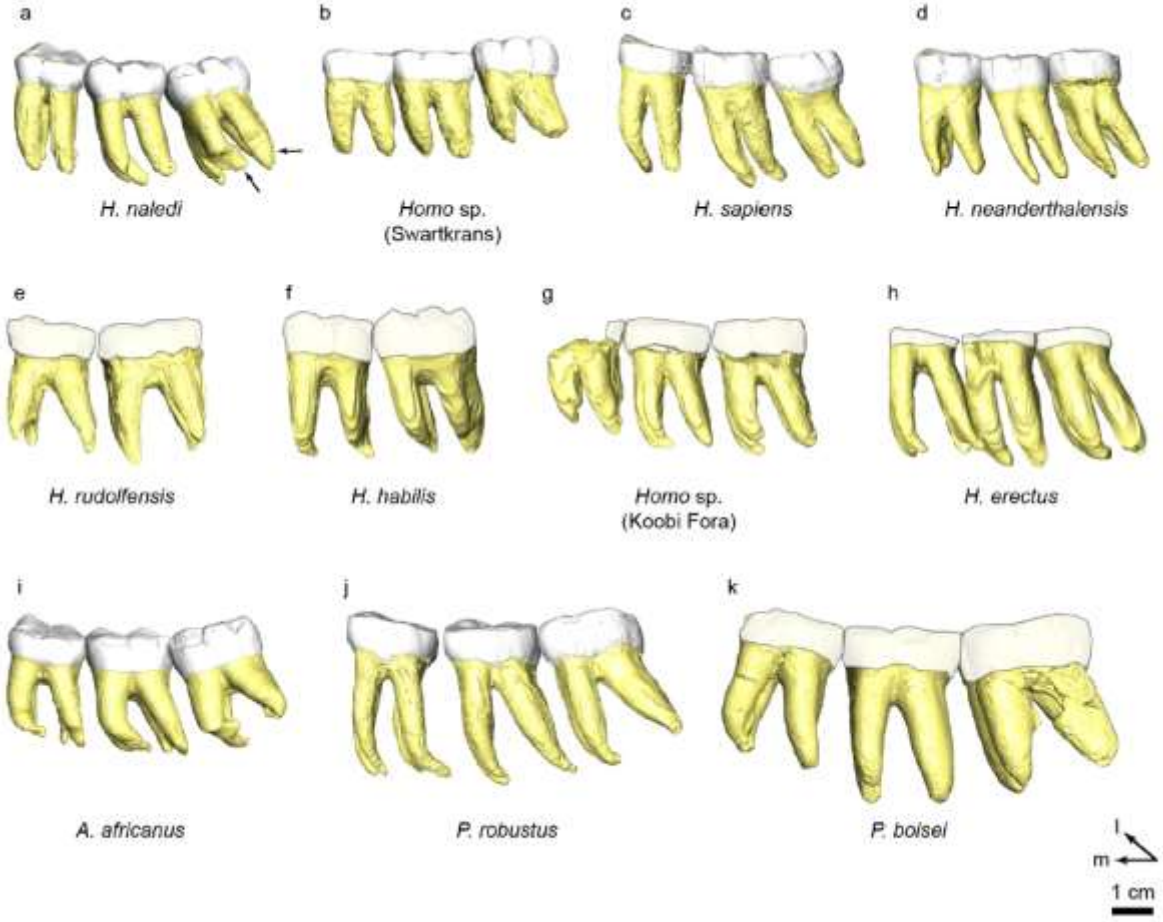
a
H. naledi
b
Homo sp.
(Swartkrans)
c
H. sapiens
d
H. neanderthalensis
e
H. rudolfensis
f
H. habilis
g
Homo sp.
(Koobi Fora)
h
H. erectus
i
A. africanus
j
P. robustus
k
P. boisei
l
m
1 cm

648

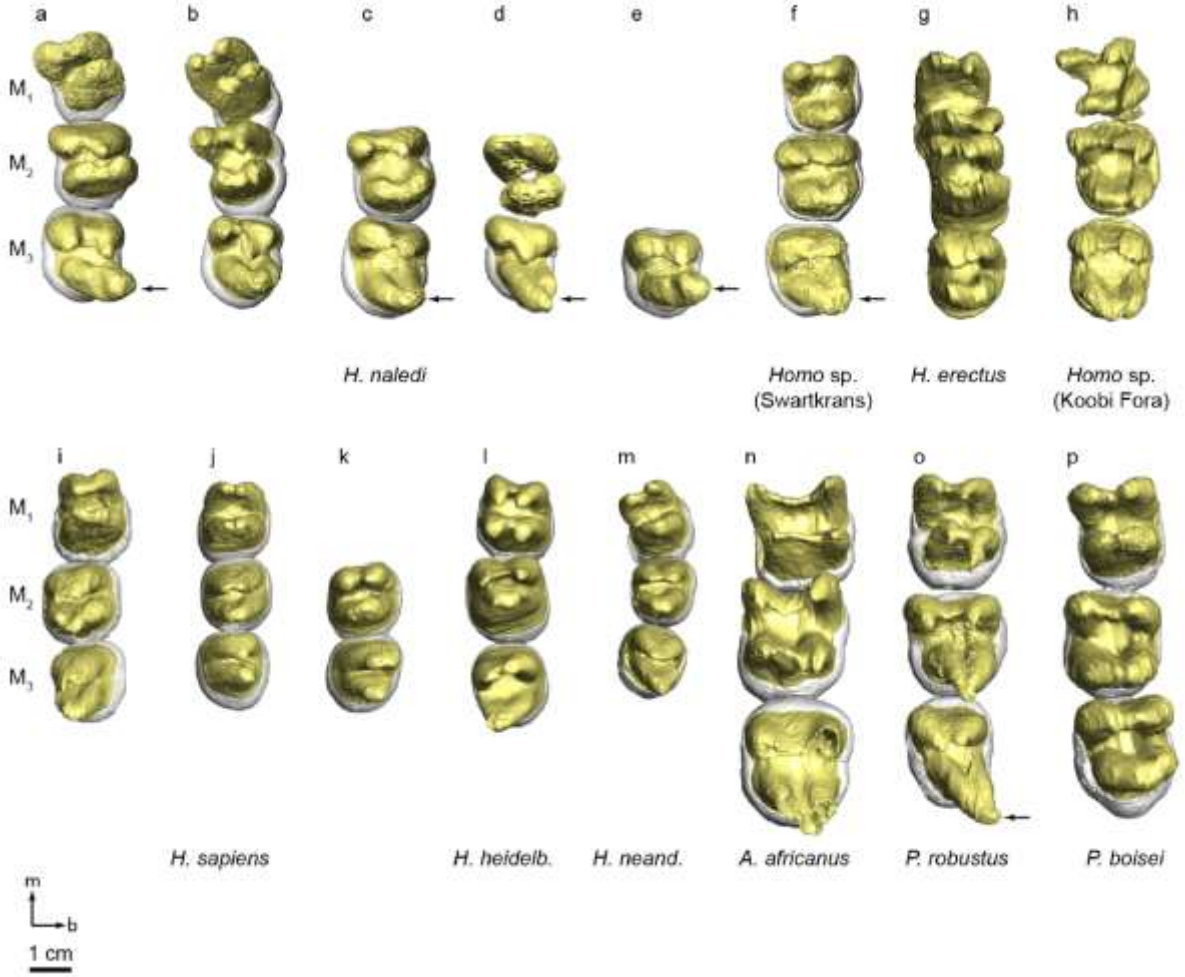
a
b
c
d
e
f
g
h
M1
M2
M3
H. naledi
Homo sp.
(Swartkrans)
H. erectus
Homo sp.
(Koobi Fora)
i
j
k
l
m
n
o
p
M1
M2
M3
H. sapiens
H. heidelb.
H. neand.
A. africanus
P. robustus
P. boisei
m
b
1 cm

649

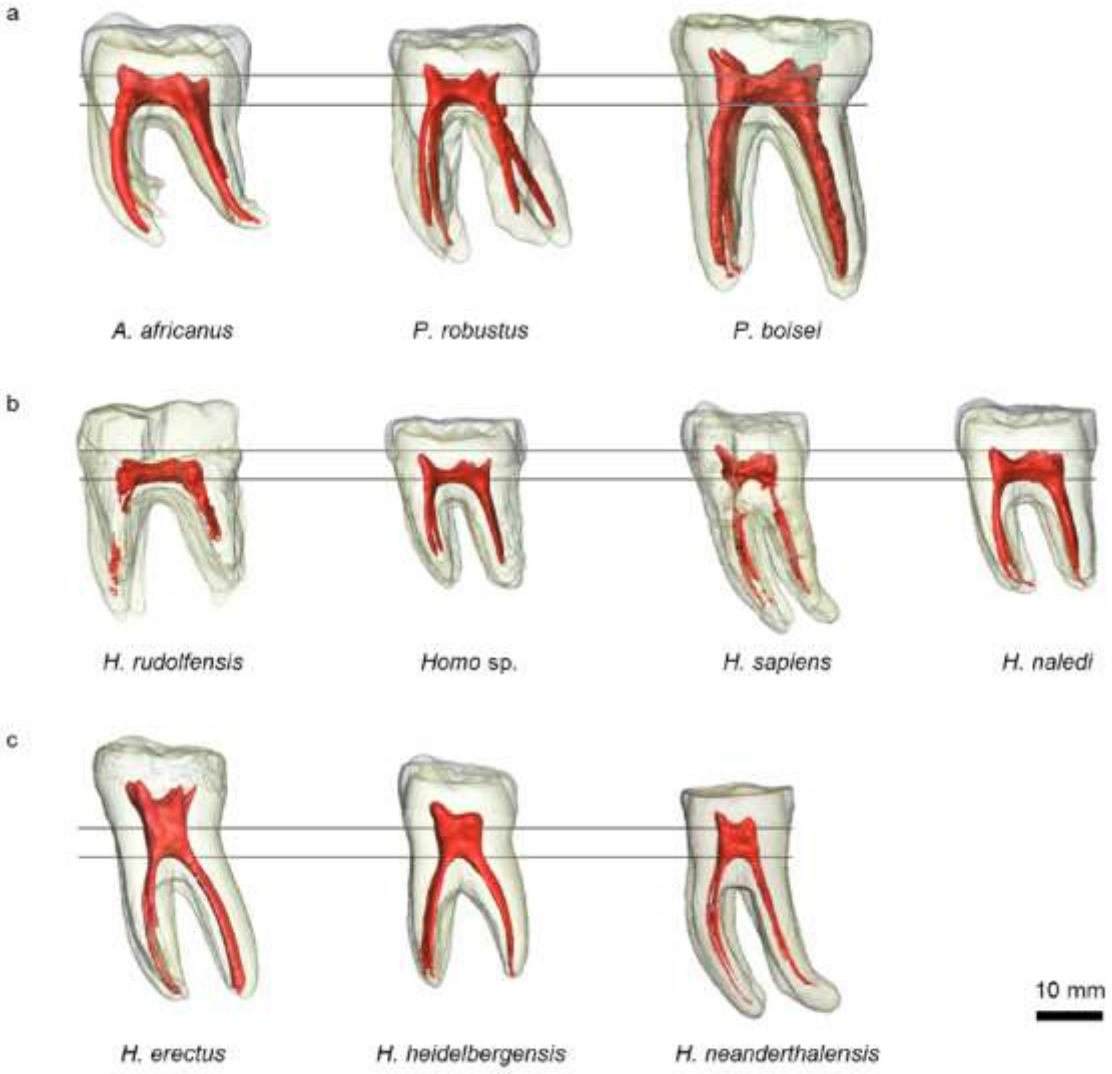
a
A. africanus
P. robustus
P. boisei
b
H. rudolfensis
Homo sp.
H. sapiens
H. naledi
c
H. erectus
H. heidelbergensis
H. neanderthalensis
10 mm

650

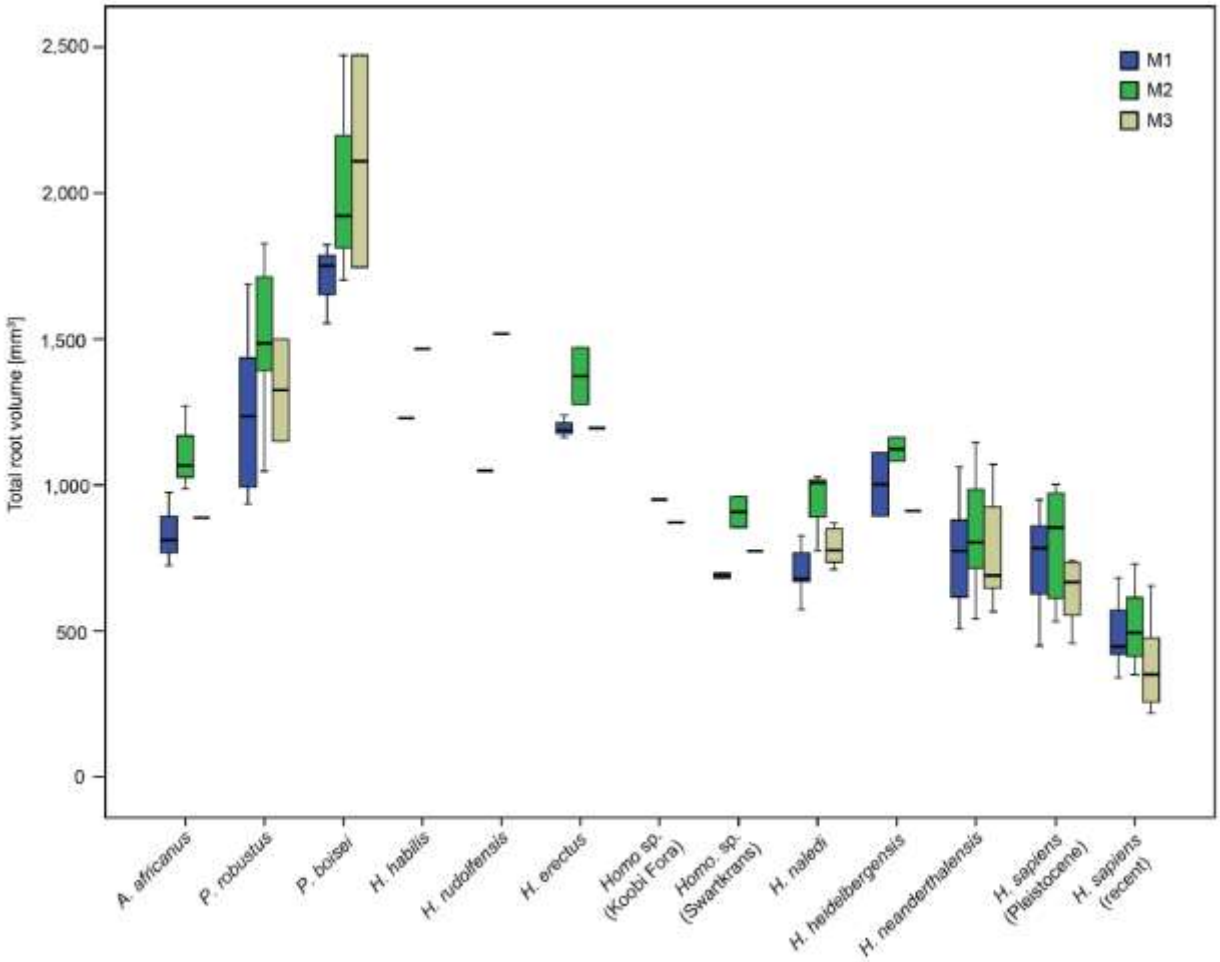
M1
M2
M3
Total root volume [mm³]
2,500
2,000
1,500
1,000
500
0
A. africanus
P. robustus
P. boisei
H. habilis
H. rudolfensis
H. erectus
Homo sp. (Koobi Fora)
Homo. sp. (Swartkrans)
H. naledi
H. heidelbergensis
H. neanderthalensis
H. sapiens (Pleistocene)
H. sapiens (recent)

651

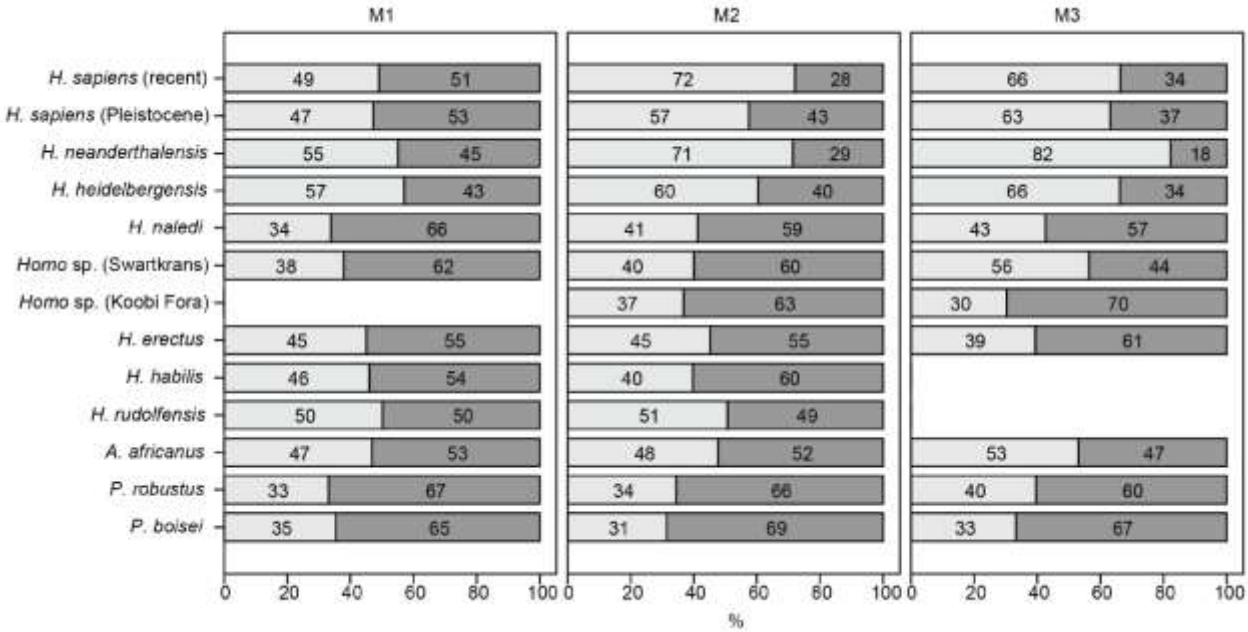
M1
M2
M3
H. sapiens (recent) 49 51 72 28 66 34
H. sapiens (Pleistocene) 47 53 57 43 63 37
H. neanderthalensis 55 45 71 29 82 18
H. heidelbergensis 57 43 60 40 66 34
H. naledi 34 66 41 59 43 57
Homo sp. (Swartkrans) 38 62 40 60 56 44
Homo sp. (Koobi Fora) 37 63 30 70
H. erectus 45 55 45 55 39 61
H. habilis 46 54 40 60
H. rudolfensis 50 50 51 49
A. africanus 47 53 48 52 53 47
P. robustus 33 67 34 66 40 60
P. boisei 35 65 31 69 33 67
0 20 40 60 80 100
%

652

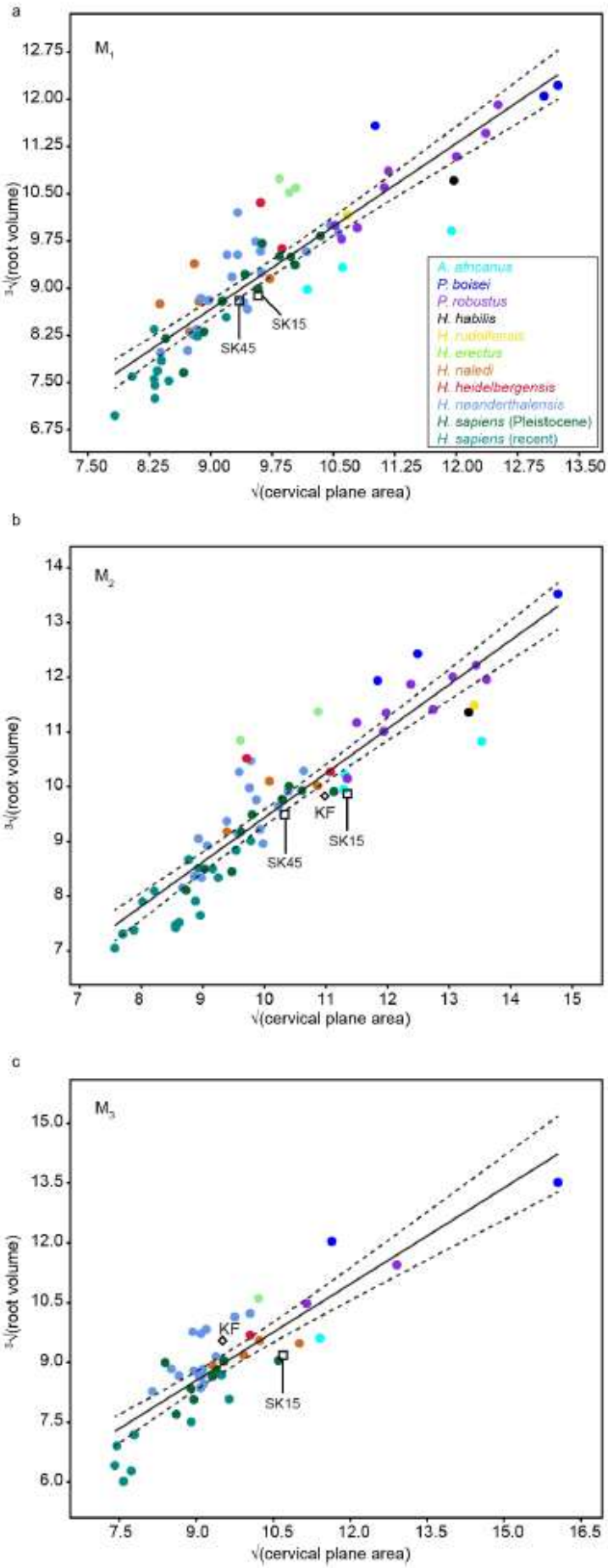
a
M1
12.75
12.00
11.25
10.50
9.75
9.00
8.25
7.50
6.75
∛(root volume)
7.50
8.25
9.00
9.75
10.50
11.25
12.00
12.75
13.50
√(cervical plane area)
SK15
SK45
A. africanus
P. boisei
P. robustus
H. habilis
H. rudolfensis
H. erectus
H. naledi
H. heidelbergensis
H. neanderthalensis
H. sapiens (Pleistocene)
H. sapiens (recent)
b
M2
14
13
12
11
10
9
8
7
∛(root volume)
7
8
9
10
11
12
13
14
15
√(cervical plane area)
KF
SK15
SK45
c
M3
15.0
13.5
12.0
10.5
9.0
7.5
6.0
∛(root volume)
7.5
9.0
10.5
12.0
13.5
15.0
16.5
√(cervical plane area)
KF
SK15

653

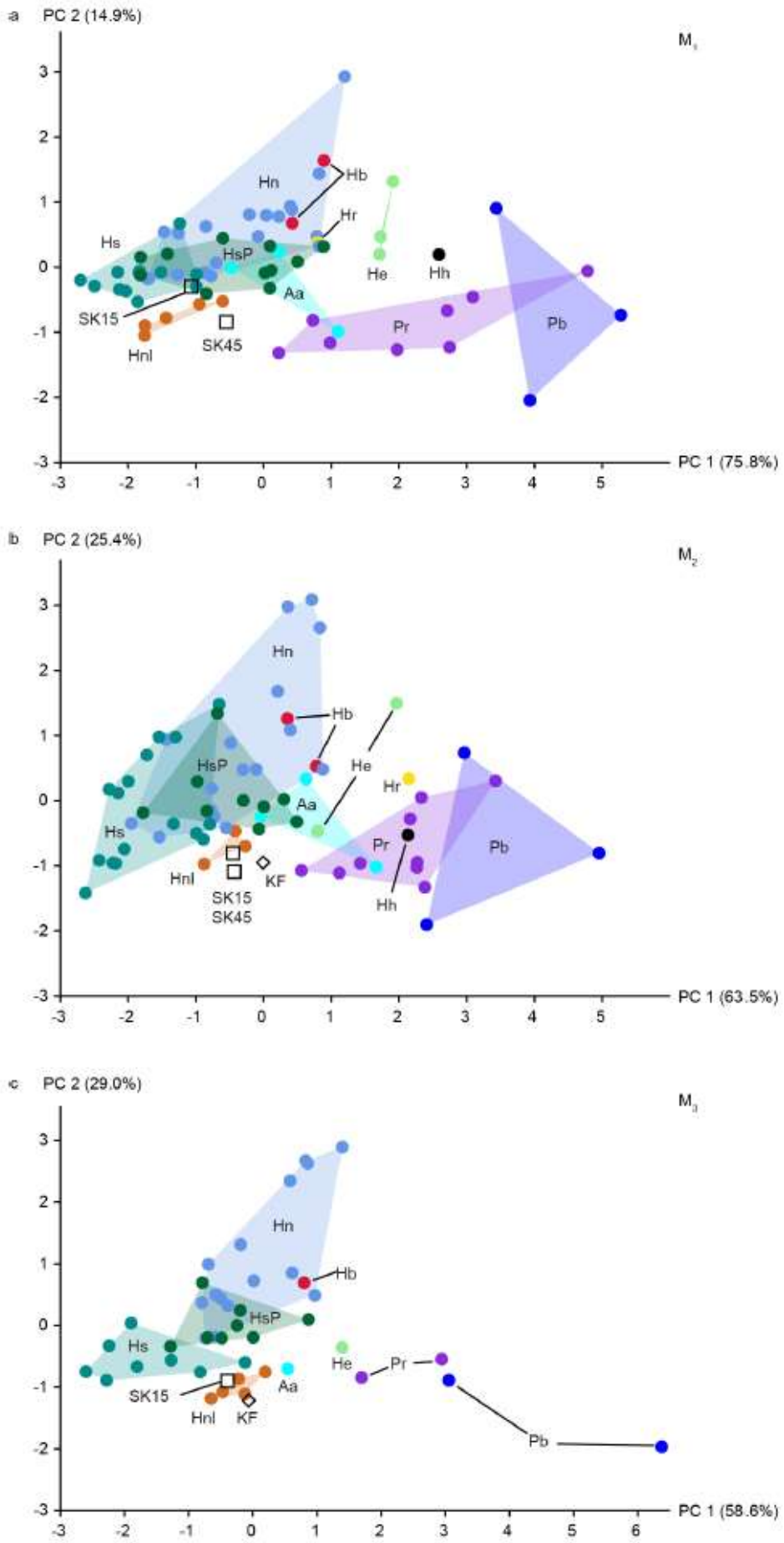
a
PC 2 (14.9%)
M1
PC 1 (75.8%)
Hn
Hb
Hr
Hs
HsP
He
Hh
Aa
SK15
SK45
Hnl
Pr
Pb
b
PC 2 (25.4%)
M2
PC 1 (63.5%)
Hn
Hb
He
HsP
Hr
Aa
Hs
Pr
Pb
Hnl
KF
SK15
SK45
Hh
c
PC 2 (29.0%)
M3
PC 1 (58.6%)
Hn
Hb
HsP
Hs
He
Pr
Aa
SK15
Hnl
KF
Pb

654

Table 1

Sample list.

Taxon	Accession number (source)	M_1	M_2	M_3	Total
Australopithecus africanus	Sts 52b, Stw 498c, Stw 404 (ESI)	3	3	1	7
Paranthropus boisei	KNM-ER 729, KNM-ER 3230, KNM-ER 15930 (NMK)	3	3	2	8
Paranthropus robustus	SK6, SK23, SK25, SK858, SK843.846a, SK1586, SK1587ab, SKW5, SKX4446, TM1600 (DNM)	8	9	2	19
Homo sp. indet. (South Africa)	SK15, SK45 (DNM), Cave of Hearths (ESI)	3	2	1	6
Homo sp. indet. (Kenya)	KNM-ER 1805 (NMK)	0	1	1	2
Homo erectus	KNM-ER 730, KNM-ER 992, KNM-WT 15000B (NMK)	3	2	1	6
Homo habilis	KNM-ER 1802 (NMK)	1	1	0	2
Homo heidelbergensis	BH1 (NMB), Mauer (GPIH)	2	2	1	5
Homo naledi	U.W. 101-001, U.W. 101-361, U.W. 101-377, U.W. 101-516, U.W. 101-582, U.W. 101-1142, U.W. 101-1261, U.W. 101-1287b (ESI)	5	3	5	13
Homo neanderthalensis	Amud 1, Tabun II C2 (TAU); and see	18	15	14	47

	Kupczik and Hublin (2010)				
Homo rudolfensis	HCRP-UR 501 (CMCK)	0	1	0	1
Homo sapiens (Pleistocene)	EQ-H71-33 (ISAM), Irhoud 11 (INSAP), Qafzeh 2, Qafzeh 9, Qafzeh 11, Qafzeh 25 (TAU), SAM AP 6242 (ISAM); and see Kupczik and Hublin (2010)	11	10	9	30
Homo sapiens (recent)	See Kupczik and Hublin (2010)	12	16	8	36

Abbreviations: BH = Mala Balanica Cave, Serbia; CMCK = Cultural and Museum Centre, Karonga, Malawi; DNM = Ditsong National Museum of Natural History, Pretoria, South Africa; ESI = Evolutionary Studies Institute, University of the Witwatersrand, Johannesburg, South Africa; EQ = Equus Cave, South Africa; GPIH = Geologisch-Paläontologisches Institut der Universität Heidelberg, Heidelberg, Germany; HCRP-UR = Hominid Corridor Research Project, Uraha, Malawi; INSAP = Institut National des Sciences de l'Archéologie et du Patrimoine, Rabat, Morocco; ISAM = Iziko South African Museum, Cape Town, South Africa; KNM-ER = National Museums of Kenya, east of Lake Turkana (formerly Lake Rudolf); KNM-WT = National Museums of Kenya, West Turkana; NMB = National Museum, Belgrade, Serbia; NMK = National Museums of Kenya, Nairobi; SK = Swartkrans, South Africa; SKW = Swartkrans, Witwatersrand, South Africa; SKX = Swartkrans, Excavations, South Africa; Sts = Sterkfontein type site; Stw = Sterkfontein, Witwatersrand, South Africa; TAU = Tel Aviv University, Israel; TM = Transvaal Museum, South Africa; U.W. = University of Witwatersrand, South Africa.

Table 2

Summary statistics (sample, mean and standard deviation).

	Taxon	*n*[a]	Root length [mm]	Cervical plane area [mm^2]	Root surface area [mm^2]	Root volume [mm^3]	Cervical root volume [mm^3]	Root branch volume [mm^3]	Volumetric bifurcation index [%]
M_1	*A. africanus*	3 (2)	14.67	119.56	707.31	836.81	391.73	445.07	47.59
			0.72	0.35	149.78	126.88	36.93	140.97	8.63
	P. boisei	3 (1)	20.15	155.81	1077.03	1709.86	604.63	1105.23	35.73
			2.41	30.04	—	139.25	113.15	220.28	8.83
	P. robustus	8 (7)	18.48	130.17	1011.16	1244.12	411.10	833.02	35.36
			2.88	18.33	217.81	269.04	137.80	143.40	11.17
	H. habilis	1	18.62	143.30	865.00	1229.35	564.97	664.38	45.96
			—	—	—	—	—	—	—

H. rudolfensis	1	14.87	113.93	826.36	1049.15	526.37	522.78	50.17
		—	—	—	—	—	—	—
H. erectus	3	19.68	98.92	893.63	1197.22	539.78	657.44	45.22
		0.50	2.08	57.01	38.80	62.89	98.63	6.60
H. naledi	5	13.20	79.37	627.61	703.12	237.81	465.31	33.52
		1.07	9.02	98.62	97.48	56.32	49.46	3.90
Homo sp. (SK)	2	14.55	89.63	696.23	690.39	262.24	428.15	37.88
		2.69	3.10	203.89	12.72	84.28	71.56	11.51
H. heidelbergensis	2	16.39	94.88	684.48	1002.91	572.15	430.76	56.71
		0.29	3.51	30.09	153.46	131.97	21.49	4.48
H. neanderthalensis [b]	19	15.63	87.43	566.52	760.15	419.22	340.93	54.62
		1.55	11.13	95.32	171.92	137.98	99.08	9.33
H. sapiens (Pleistocene) [b]	11	15.38	89.75	576.36	742.65	351.35	391.30	48.29

		(10)	1.79	11.25	108.48	162.20	55.86	117.84	6.51
	H. sapiens (recent) [b]	12	13.69	71.76	424.62	485.02	237.90	247.12	49.27
			0.94	7.02	65.58	104.04	58.52	70.09	7.25
M_2	*A. africanus*	2	15.89	146.11	834.49	1108.00	528.78	579.22	48.51
			1.24	31.90	140.61	146.61	63.61	189.60	9.98
	P. boisei	3 (1)	20.16	171.41	1154.19	2033.11	637.52	1395.58	30.86
			0.65	41.25	—	395.62	305.33	324.09	13.89
	P. robustus	9 (8)	18.22	155.49	1107.32	1518.66	522.39	996.28	34.06
			1.56	20.50	196.49	244.97	144.06	148.94	5.45
	H. habilis	1	17.48	177.50	959.59	1466.41	582.31	884.10	39.71
			—	—	—	—	—	—	—
	H. rudolfensis	1	16.72	179.89	1056.66	1518.19	769.47	748.72	50.68
			—	—	—	—	—	—	—

H. erectus	2	19.79	105.19	957.35	1373.50	621.59	751.92	44.42
		0.99	18.28	24.52	138.49	288.86	150.37	16.55
H. naledi	3	14.63	102.62	704.33	936.85	386.37	550.47	40.78
		1.09	14.92	38.82	140.85	109.79	69.81	7.05
Homo sp. (SK)	2	14.15	117.70	740.51	907.66	363.45	544.21	39.69
		1.82	15.63	111.17	74.68	107.41	32.72	8.57
Homo sp. (KF)	1	15.64	120.56	956.46	950.19	348.67	601.52	36.69
		—	—	—	—	—	—	—
H. heidelbergensis	2	17.39	108.40	693.44	1123.01	678.91	444.10	60.33
		0.45	19.98	14.62	57.99	92.89	34.90	5.15
H. neanderthalensis [b]	16	16.47	92.50	551.20	835.19	596.53	238.66	70.65
		2.10	11.14	100.22	190.02	236.46	168.74	18.99
H. sapiens (Pleistocene) [b]	9	16.01	98.53	577.19	807.06	463.78	343.28	60.57

			1.37	15.40	120.02	183.45	64.45	197.60	18.37
	H. sapiens (recent) [b]	16	13.99	71.66	397.32	464.55	340.23	124.32	75.75
			1.74	11.10	88.11	118.18	146.69	142.36	25.21
M_3	*A. africanus*	1	13.79	130.24	683.14	887.66	470.74	416.92	53.03
			—	—	—	—	—	—	—
	P. boisei	2 (1)	19.10	196.46	1111.63	2109.38	701.21	1408.17	33.19
			0.04	86.32	—	513.52	179.40	334.12	0.42
	P. robustus	2	17.93	145.51	935.72	1324.93	523.52	801.41	38.83
			0.33	29.92	100.06	247.50	194.16	53.34	7.40
	H. erectus	1	17.98	104.19	845.74	1194.73	470.77	723.96	39.40
			—	—	—	—	—	—	—
	H. naledi	7	14.55	101.04	585.93	864.51	393.85	470.66	45.31
			2.27	11.13	36.24	162.85	122.75	128.10	10.81

Homo sp. (SK)	1	11.37	114.18	599.31	773.90	436.65	337.25	56.42
		—	—	—	—	—	—	—
Homo sp. (KF)	1	14.55	90.52	1130.92	871.60	263.31	608.29	30.21
		—	—	—	—	—	—	—
H. heidelbergensis	1	17.40	101.09	586.30	910.96	602.38	308.58	66.13
		—	—	—	—	—	—	—
H. neanderthalensis [b]	15	16.39	82.58	488.53	763.08	627.84	135.24	80.66
		2.22	8.32	69.48	171.65	248.58	138.99	18.04
H. sapiens (Pleistocene) [b]	8	15.30	85.25	458.46	638.95	403.45	235.50	64.62
		1.62	13.02	73.29	107.08	61.65	115.67	15.11
H. sapiens (recent) [b]	8	12.49	68.82	322.33	380.02	251.96	128.06	72.84
		1.82	16.00	122.05	150.80	50.85	137.93	23.73

[a] Sample size in parenthesis for RSA only.

[b] Data partially from Kupczik and Hublin (2010).

Table 3

Ordinary least squares regression statistics for cervical plane area against root surface area (A) and root volume (V) in hominin mandibular molars.

Molar	A/V	*n*	Pearson's r correlation	Slope	Confidence intervals [b]
M_1	Area	65	0.87 [a]	1.28	1.09, 1.47
	Vol	69	0.90 [a]	0.88	0.77, 0.98
M_2	Area	65	0.90 [a]	1.24	1.09, 1.37
	Vol	68	0.91 [a]	0.81	0.72, 0.90
M_3	Area	44	0.82 [a]	1.31	1.02, 1.62
	Vol	45	0.87 [a]	0.81	0.56, 0.93

[a] $p < 0.0001$, permutation test ($n = 9999$).

[b] 95% bootstrapped ($n = 1999$).

Table 4

Principal components analysis (PCA) component loadings.

Molar	Variable	PC1	PC2	PC3
M_1	RL	0.511	0.180	-0.789
	CPA	0.528	-0.292	0.504
	V_{cervix}	0.449	0.762	0.351
	V_{branch}	0.510	-0.549	-0.040
	% variance	75.842	14.9	7.366
M_2	RL	0.527	0.241	-0.772
	CPA	0.569	-0.231	0.518
	V_{cervix}	0.342	0.797	0.367
	V_{branch}	0.531	-0.504	-0.025
	% variance	63.511	25.376	9.76
M_3	RL	0.498	0.384	-0.739
	CPA	0.582	-0.295	0.440
	V_{cervix}	0.383	0.684	0.489
	V_{branch}	0.516	-0.546	-0.145
	% variance	58.547	28.993	11.176

Abbreviations: CPA = cervical plane area; ; RL = root length; V_{branch} = root branch volume; V_{cervix} = cervical root volume.

686